Low Temperature Physics/Fizika Nizkikh Temperatur, 2012, v. 38, No. 7, pp. 715–727

Low-dimensional magnetism of spin-½ chain systems α- and β-$TeVO_4$: a comparative study

V. Gnezdilov[1,2], P. Lemmens[2], D. Wulferding[2], Yu. Pashkevich[3], K. Lamonova[3], K.-Y. Choi[4], O. Afanasiev[1], S. Gnatchenko[1], and H. Berger[5]

[1]*B. Verkin Institute for Low Temperature Physics and Engineering of the National Academy of Sciences of Ukraine*
47 Lenin Ave., Kharkov 61103, Ukraine
E-mail: gnezdilov@ilt.kharkov.ua

[2]*Institute for Condensed Matter Physics, Braunschweig University of Technology*
Braunschweig D–38106, Germany

[3]*Donetsk O.O. Galkin Institute of Physics and Engineering of National Academy of Sciences of Ukraine*
72 R. Luxemburg Str., Donetsk 83114, Ukraine

[4]*Department of Physics, Chung-Ang University, 221 Huksuk-Dong, Dongjak-Gu, Seoul 156–756, Republic of Korea*

[5]*Inst. Phys. Mat. Complexe, EPFL, Lausanne CH–1015, Switzerland*

Received April 4, 2012

We present a comparative study of the low-dimensional compounds α- and β-$TeVO_4$. Our data clearly show that the change in the local coordination geometry of V^{4+} ions comparing α- and β-$TeVO_4$ leads to a drastic differences in the magnetic properties. Despite sharing the same crystal structure, the two compounds realize different magnetic exchange topologies. Both compounds exhibit a transition from ferro- to antiferromagnetic correlations with decreasing temperature. This effect however is driven by different mechanisms for both compounds. Additionally, a dimensional crossover is found in β-$TeVO_4$.

PACS: 75.40.Gb Dynamic properties (dynamic susceptibility, spin waves, spin diffusion, dynamic scaling, etc.);
63.20.–e Phonons in crystal lattices;
78.30.–j Infrared and Raman spectra;
75.50.–y Studies of specific magnetic materials.

Keywords: Raman scattering, low-dimensional magnetic systems, phononic and magnetic excitations.

1. Introduction

A variety of compounds has been synthesized to date which can serve as model systems for the investigation of quantum spin systems with a one-dimensional (1D) arrangement of spins. Vanadium oxides hold a special place among them due to the variety of bonding patterns (resulting in octahedral, tetrahedral, trigonal or square pyramidal coordinations) that vanadium ions can exhibit together with different possible oxidation states. Of particular interest are vanadium oxides with V^{4+} (S = 1/2) magnetic centers as with the lowest spin value the strongest quantum fluctuations are expected.

In general, the signs and magnitudes of spin exchange interactions depend on the geometry of the spin exchange paths [1]. The dominant interaction in a chain of corner-sharing vanadium oxide units is the nearest-neighbor (NN) superexchange. Linear or nearly linear V–O–V bonds along the spin chains give rise to a large antiferromagnetic (AFM) NN coupling. In an edge-sharing chain the NN coupling is more than an order of magnitude smaller than in the corner-sharing case. Its sign and absolute value depend sensitively on the V–O–V angle and the V–O distance.

The next-nearest-neighbor (NNN) interaction in corner-sharing chains has a small magnitude relative to the NN interaction and usually can be neglected. In the edge-sharing case, the NNN interaction via V–O–O–V is generally AFM and despite its small magnitude, has a pronounced effect on the system's physical properties since NN coupling is small as well.

At low temperatures, besides intrachain NN and NNN couplings, other forms of interactions (e.g., strong enough

interchaing coupling or spin-phonon interaction) become relevant, driving a system to various phases with decreasing temperature.

The compound $TeVO_4$ offers a unique opportunity: (i) it has two crystalline structures, α and β with the same crystallographic symmetry but with a different geometry of spin exchange pathways; (ii) the lone pair cations Te^{4+} are very important players involved in lowering the dimensionality of crystal structure. Here, we present an investigation of the phononic and magnetic excitations in both crystalline forms studied by inelastic light scattering (Raman scattering). This technique has proven to be extremely powerful to probe magnetic excitations and spin-lattice interactions in a low-dimensional spin system with very high precision [2]. In addition, the temperature dependencies of magnetic susceptibility $\chi(T)$, specific heat $C_p(T)$, orbital state, and g-factors were analyzed.

2. Experimental details

Single crystals of α/β-$TeVO_4$ were grown as described previously [3,4]. Large samples with well-defined growth edges were oriented via x-ray Laue diffractometry. Raman scattering measurements were performed in quasi backscattering geometry using λ = 514.5 nm Ar^+ and λ = = 532.1 nm solid state lasers. The laser power of <10 mW was focused to a 0.1 mm diameter spot on the sample surface. Spectra of the scattered radiation were collected via a triple spectrometer (Dilor-XY–500) and recorded by a nitrogen-cooled CCD detector (Horiba Jobin-Yvon, Spectrum One CCD–3000V) with a spectral resolution of ~ 0.5 cm^{-1}.

Magnetic susceptibility $\chi(T)$ was measured in the range 1.85 K ≤ T ≤ 400 K at magnetic fields of 0.001–5 T by a superconducting quantum interference device (SQUID) magnetometer (Quantum Design). Specific-heat measurements were performed using a physical property measurement system (PPMS) calorimeter (Quantum Design) using the relaxation method.

3. Results and discussion

3.1. Crystal structure

The compound $TeVO_4$ can be prepared in two different crystalline structures with a reversible polymorphic transformation at 650 °C (α↔β) [3,4]. Both crystallize in the monoclinic system, space group $P2_1/c$ (C_{2h}^5, № 14, $Z = 4$) with the room temperature lattice parameters a = 5.099 Å, b = 4.93 Å, c = 12.672 Å, β = 105.85°, and a = 4.379 Å, b = 13.502 Å, c = 5.446 Å, β = 91.72° for α- and β-$TeVO_4$, respectively [3,4]. The crystal structures of α- and β-$TeVO_4$ are shown in Fig. 1,*a,c*.

The structure of α-$TeVO_4$ consists of $\left[VO_4\right]_n^{4n-}$ zigzag chains along to the b axis formed by distorted edge sharing VO_6 octahedra. The crystal structure of β-$TeVO_4$ also consists of zigzag chains parallel to the c axis formed by slightly distorted square pyramids of VO_5 sharing corners. There are two identical zigzag chains, with the apices of the square pyramids alternating below and above the bc plane. In both structures the lone pair cation Te^{4+} leads to a magnetic separation of chains.

Figure 1,*b,d* shows the exchange topology of α/β-$TeVO_4$. For α-$TeVO_4$ the NN V–V bond in the chains has alternating V–V distances (2.83 Å/3.27 Å) and V–O–V angles (97.07°/107.29°). In contrast, for β-$TeVO_4$ the single NN exchange path for the V^{4+} ions has a V–V distance of 3.64 Å and a V–O–V angle of 133.7°. The nearest V–V distances perpendicular to the chain direction are 5.099/5.696 Å along the a/c axes and 4.3790/4.9149 Å along a/b axes in α- and β-$TeVO_4$, respectively.

In Refs. 5,6 the dependence of the magnetic interactions on the Me–O–Me angle was analyzed. According to de Graaf *et al*. [6], the angle at which FM exchange interaction reaches its maximum is close to 97°, while the critical angle at which the exchange interaction changes its sign from FM to AFM is close to 104°. From geometrical considerations, it can be expected that the NN exchange interactions in α-$TeVO_4$ have different magnitudes (and possibly signs) due to the difference in V–V distances and V–O–V angles. Beside, NNN supersuperexchange interaction, which originates from the V–O–O–V path, can play an important role in the magnetic properties of this compound. In the β-$TeVO_4$ a V–O–V angle of 133.7° is far from the critical value of 104°, therefore only the AFM NN intrachain coupling interaction is expected. In addition, the two nearest neighbors V–O–V intrachain exchange paths (V_n–O–V_{n+1} and V_{n-1}–O–V_n) are situated in different planes. This structural feature is a necessary prerequisite for the nonzero Dzyaloshinskii–Moriya (DM) interaction.

3.2. Magnetic susceptibility, specific heat, V^{4+} orbital state, and g-factors

The magnetic susceptibility $\chi(T)$ of α- and β-$TeVO_4$ measured along and perpendicular to the effective chain directions shows a noticeable axial anisotropy of magnetic properties with respect to the chain directions. Figure 2,*a* presents $\chi(T)$ measured along the chain directions. The main features of the $\chi(T)$ curves are the presence of a maximum characteristic for low-dimensional spin systems at $T_{\chi_{max}}$ = 18.3 K and $T_{\chi_{max}}$ = 14.4 K (a temperature at which $d\chi/dT$ = 0) for α- and β-$TeVO_4$, respectively. A Curie–Weiss fit to the high-temperature susceptibility yields a Curie constant C = 0.344 emu·K·mol^{-1} and a positive Curie–Weiss temperature of Θ_{CW} = +25.6 K for magnetic fields applied along the b direction in α-$TeVO_4$. For magnetic fields within the ac plane, we find C = = 0.346 emu·K·mol^{-1} and Θ_{CW} = +24.8 K. In the case of β-$TeVO_4$, a Curie–Weiss fit gives C = 0.362 emu·K·mol^{-1}, Θ_{CW} = +1.7 K ($H \| c$), C = 0.361 emu·K·mol^{-1}, Θ_{CW} = = +1.6 K ($H \| a$), and C = 0.385 emu·K·mol^{-1}, Θ_{CW} = +4.4 K ($H \| b$). A positive Curie–Weiss temperature indicates pre-

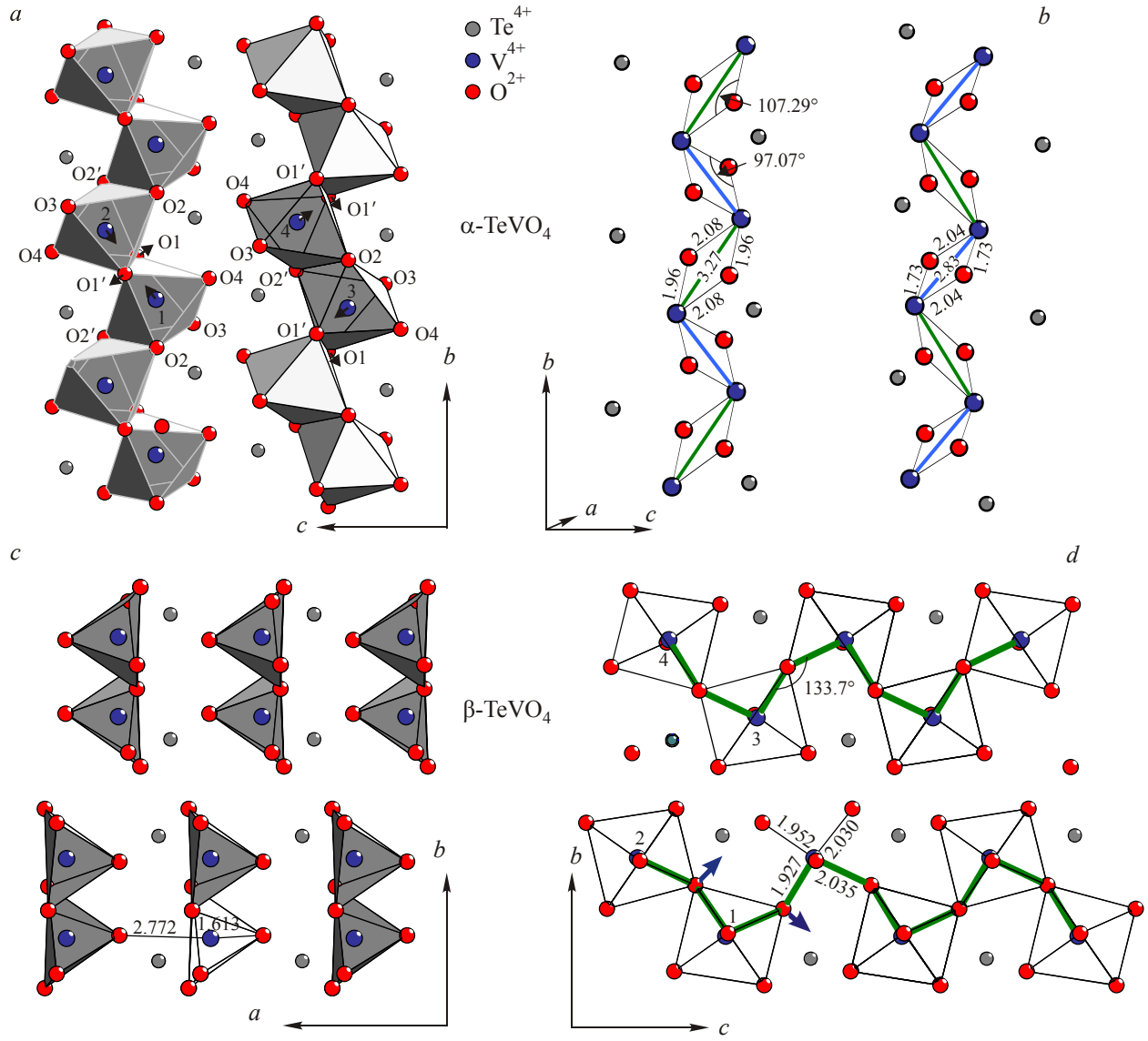

Fig. 1. (Color oline) Projections of the lattice structure of α- and β-$TeVO_4$ (*a*), (*c*). Chains along the *b* axis in (*a*) are formed by rows of VO_6 octahedra sharing edges. The vanadium ions are labeled from 1 to 4. Chains along the *c* axis in (*c*) are formed by rows of corner sharing VO_5 pyramids. Arrows show possible lattice distortions which change the angles of V–O–V bonds at T close to T^*. Schematic drawing of V^{4+}- and O^{2-}-ion positions in α- and β-$TeVO_4$ (*b*), (*d*). The thick lines denote V–O–V magnetic bonds for α-$TeVO_4$ (green and blue) and for β-$TeVO_4$ (green). The vanadium ions in β-$TeVO_4$ occupy the following coordinates: (1) [0.68, 0.16, 0.66], (2) [0.68, 0.34, 0.16], (3) [0.32, 0.66, 0.84], and (4) [0.32, 0.84, 0.34]. The arrows in (*d*) denote projections of Dzyaloshinskii–Moriya vectors on the *bc* plane.

dominant ferromagnetic spin-spin correlations at high temperatures down to the crossover temperature T^*, i.e., the center of a broad (~40 K wide) temperature region in the $1/\chi(T)$ plot with a different slope above and below it. In Refs. 7, 8, $T^*_{\alpha/\beta} = 85/130$ K for α-/β-$TeVO_4$ was related to a modification of the magnetic exchange interaction along the zigzag chain.

At low temperatures magnetic susceptibility shows kinks at $T_c^{\alpha-TeVO_4} = 16.13$ K and $T_c^{\beta-TeVO_4} = 4.65$ K which may indicate that the compounds undergo a magnetic phase transition into a long-range ordered phase. The kinks in $\chi(T)$ become more evident in a plot of $d\chi/dT$ vs T as sharp peaks shown in Fig. 2,*b*. Beside, two additional features at 2.26 and 3.28 K are present on the $d\chi/dT$ vs T plot of β-$TeVO_4$. These features might be interpreted as a further modification of the magnetically ordered phase [8].

The zero-field specific heat $C_p(T)$ (not shown here) shows λ-shaped peaks with the maximum at $T^{C_p}_{max} = 16.9$ and 4.64 K for α- and β-$TeVO_4$, respectively. These characteristic temperatures nearly coincide with the temperatures of maximum in $d\chi/dT$ indicating that the sharp peaks in $C_p(T)$ can be attributed to magnetic phase transitions. Detailed analysis for the α-$TeVO_4$ specific heat behavior is presented in Ref. 7 while for the β-$TeVO_4$ it will be published separately.

In Ref. 7 an analysis of the magnetic susceptibility and the specific heat of α-$TeVO_4$ was performed in terms of a single spin-1/2 chain model. The best qualitative agree-

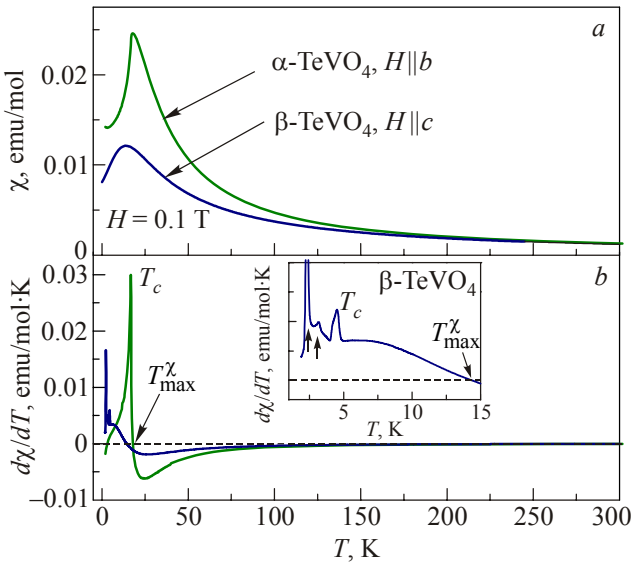

Fig. 2. Temperature dependence of the magnetic susceptibility of α- and β-$TeVO_4$ measured in a magnetic field H = 0.1 T applied along the chain directions (*a*). $d\chi/dT$ versus T; the magnetic phase transitions are manifested as sharp peaks at T_c = 16 K (α-$TeVO_4$) and T_c = 4.6 K (β-$TeVO_4$) in $d\chi/dT$ (*b*). The inset in (*b*) shows low-temperature part of $d\chi/dT$ for β-$TeVO_4$.

ment with the experiment was obtained for the FM alternating NN couplings and AFM NNN couplings with a weak easy-plane magnetic anisotropy. The Hamiltonian of a single spin-1/2 chain of V^{4+} ions can be written as:

$$H = \sum_{i=1}^{N}\left[J_1^z S_{2i}^z S_{2i-1}^z + J_1^{xy}(S_{2i}^x S_{2i-1}^x + S_{2i}^y S_{2i-1}^y)\right] + \sum_{i=1}^{N}\left[J_1^{'z} S_{2i}^z S_{2i+1}^z + J_1^{'xy}(S_{2i}^x S_{2i+1}^x + S_{2i}^y S_{2i+1}^y)\right] + \sum_{i=1}^{N}\left[J_2^z S_{2i}^z S_{2i-1}^z S_{2i+1}^z + J_2^{xy}(S_{2i-1}^x S_{2i+1}^x + S_{2i-1}^y S_{2i+1}^y)\right] + \sum_{i=1}^{N}\left[J_2^z S_{2i}^z S_{2i+2}^z + J_2^{xy}(S_{2i}^x S_{2i+2}^x + S_{2i}^y S_{2i+2}^y)\right]. \quad (1)$$

Here J_1^z, J_1^{xy}, $J_1^{'z}$, and $J_1^{'xy}$ are the alternating exchange constants between the nearest-neighbor spins, J_2^z and J_2^{xy} are the exchange constants between next-nearest neighbor spins, and S_i denote operators of spin 1/2 at the ith site of the chain. Because of the alternation of the lattice spacing between nearest V^{4+} ions, the model takes into account the small possible alternation of the NN exchange couplings. A small uniaxial magnetic anisotropy of the exchange interactions $J^z \neq J^{xy}$, which follows from the different temperature dependences of the magnetic susceptibility of the system along and perpendicular to the effective chains direction was introduced as well.

The magnetic properties of β-$TeVO_4$ were analyzed within the framework of a few microscopic models [8]. The best qualitative agreement with the magnetic susceptibility data was obtained in the wide temperature range for the Heisenberg model on a one-dimensional spin-1/2 chain,

$$H = J\sum_{i=1}^{N}\mathbf{S}_i \cdot \mathbf{S}_{i+1}, \quad (2)$$

with the single intrachain antiferromagnetic coupling constant J/k_B = (21.4 ± 0.2) K. It was determined that the attempt to extend the 1D spin model leads only to small strengths of other exchange integrals (AFM or FM in nature) for this quasi-one-dimensional antiferromagnet. Below we extend this model to describe the possible long rang ordered state in β-$TeVO_4$.

The most intriguing feature of both α- and β-$TeVO_4$ compounds is the change of the spin-spin correlations from ferromagnetic to antiferromagnetic with lowering temperature through T^*. In the α-$TeVO_4$ we attribute this behavior to a temperature dependent competition between FM and AFM exchanges along chains which are separately realized on two (short and long) types of NN magnetic bonds (see Fig. 1,*b*) [7]. This explanation does not work for β-$TeVO_4$, where only a single exchange pathway is realized. However, according to the Goodenough–Kanamori–Anderson rules, the crossover from AFM to FM type of bonding can be induced by an orbital reordering in the system. One can expect that the source of an orbital instability in β-$TeVO_4$ can be connected with a change of the anomalously close distance V–O_{ap} between the vanadium ion and the apical oxygen ion in the VO_5 pyramidal complexes. Indeed, using a modified crystal field (MCF) approach [9] and crystallographic data [4] we found that a modest shift δ of the vanadium ion away from the apical oxygen drastically changes its orbital state. Some results of our calculations of the V^{4+} orbital ground states (wave functions) for the first Kramer's doublet are shown below, for three different distances: I. V–O_{ap} = 1.613 Å (δ = 0); II. V–O_{ap} = 1.663 Å (δ = 0.05 Å); and III. V–O_{ap} = 1.863 Å (δ = 0.25Å):

$$\begin{aligned}\Psi_{\mathrm{I}} &= 0.75\cdot\Psi_{xy} + 0.43\cdot\Psi_{x^2-y^2} + 0.42\cdot\Psi_{3z^2-r^2} + \\ &\quad + 0.25\cdot\Psi_{xz}\ldots; \\ \Psi_{\mathrm{II}} &= 0.55\cdot\Psi_{3z^2-r^2} + 0.5\cdot\Psi_{xy} + 0.47\cdot\Psi_{x^2-y^2} + \\ &\quad + 0.33\cdot\Psi_{yz} + 0.32\cdot\Psi_{xz}\ldots; \\ \Psi_{\mathrm{III}} &= 0.83\cdot\Psi_{yz} + 0.47\cdot\Psi_{xy} + 0.22\cdot\Psi_{3z^2-r^2}\ldots\end{aligned} \quad (3)$$

The contributions from *d* orbitals with coefficients less then 0.2 as well as the up- and down spin indices ↑,↓ are omitted for clarity. We use a rectangular coordinate systems with $OX\|a$ axis and $OY\|b$ axis and the oxygen valence state Z_O = –2. We also assumed that for all cases the oxygen ions in the VO_5 pyramid do not shift. The mix of different orbital states is caused by the highly distorted VO_5 pyramidal complex [3,4]. Note, that the first distance (δ = 0) is taken from crystallographic data which were obtained at room temperature [4].

As follows from (3), the gradual (or temperature induced) outward motion of vanadium ion leads to the orbital rotation from mostly *ab* plane towards *bc* plane. Moreover, the explicit results (3) support the scenario of an orbital reordering mechanism of the FM–AFM spin-spin interaction crossover in β-$TeVO_4$. Indeed, at high temperatures (case I, δ = 0), the mostly d_{xy} orbital state, being perpendicular to the chain direction, has small overlap with the *p* orbitals of the intermediate oxygen from the V–O–V path. Therefore it creates a weak ferromagnetic intrachain interaction. Meanwhile, the mostly d_{yz} orbital (case III, δ = 0.25Å) has a considerably larger overlap with the oxygen *p* orbitals leading to an antiferromagnetic exchange. Our Raman spectra support this scenario, as shown below.

To obtain the orbital ground state we should know the magnitude of the metal ion nuclear effective charge Z_{eff} which is the main parameter of the MCF theory [10]. The theory becomes self-consistent if this parameter can be restored independently from experiments [11]. The results (3) have been obtained for $Z_{\text{eff}} = 3.4|e|$ (the Slater estimation for free V^{4+} ion is $5|e|$) [12]. We deduced this value of Z_{eff} using the experimental data for *g*-factors taken at high temperatures [8]. Surprisingly, in spite of the highly distorted VO_5 pyramid, we obtained a very nice coincidence between experimental ($g_a = 1.962$; $g_b = 2.027$; $g_c = 1.965$) and theoretical ($g_a^{\text{th}} = 1.9625$; $g_b^{\text{th}} = 1.9921$; $g_c^{\text{th}} = 1.9649$) data for the case III of vanadium ion shift (δ = 0.25 Å). The shifts with lower magnitudes create smaller values of *g*-factors, while a larger magnitude of shifts does not strongly affect the *g*-factors values. At least our theory could not achieve the low temperature experimental values ($g_a = 2.185$; $g_b = 2.28$; $g_c = 2.20$) [8] at any reasonable shifts of the V^{4+} ion and at the given coordination of oxygen ions. Furthermore, the increase of the $V–O_{ap}$ distance up to δ = 0.5 Å does not affect the orbital state which remains mostly d_{yz} (i.e., similar to the Ψ_{III}).

3.3. Symmetry analysis and possible types of long range magnetic order

To perform a symmetry analysis of possible long range magnetically ordered states in α- and β-$TeVO_4$, we follow the approach of Bertaut [13] and Izyumov and Naish [14]. Both modifications of the $TeVO_4$ have the same symmetry (space group $P2_1/c$) and the primitive cells contain four V^{4+} ions on 4*e* positions, with their coordinations shown in Fig. 1. We introduce magnetic modes as linear combinations of sublattice spins S_γ, where γ denotes a particular sublattice:

$$\mathbf{F} = \mathbf{S}_1 + \mathbf{S}_2 + \mathbf{S}_3 + \mathbf{S}_4 = \mathbf{m}_1 + \mathbf{m}_2,$$

$$\mathbf{L}_1 = \mathbf{S}_1 + \mathbf{S}_2 - \mathbf{S}_3 - \mathbf{S}_4 = \mathbf{m}_1 - \mathbf{m}_2,$$

$$\mathbf{L}_2 = \mathbf{S}_1 - \mathbf{S}_2 + \mathbf{S}_3 - \mathbf{S}_4 = \mathbf{l}_1 + \mathbf{l}_2,$$

$$\mathbf{L}_3 = \mathbf{S}_1 - \mathbf{S}_2 - \mathbf{S}_3 + \mathbf{S}_4 = \mathbf{l}_1 - \mathbf{l}_2.$$

Here $\mathbf{l}_1 = \mathbf{S}_1 - \mathbf{S}_2$ and $\mathbf{l}_2 = \mathbf{S}_3 - \mathbf{S}_4$ denote AFM vectors and $\mathbf{m}_1 = \mathbf{S}_1 + \mathbf{S}_2$ and $\mathbf{m}_2 = \mathbf{S}_3 + \mathbf{S}_4$ the sublattice magnetizations of neighboring chains. **F** is the "ferromagnetism vector" of the crystal. $\mathbf{L}_1$ is determined by the difference of the ferromagnetism vectors of neighboring chains. Hence, only $\mathbf{L}_2$ and $\mathbf{L}_3$ represent the intrachain AFM ordering. For a second order magnetic phase transition the possible magnetic structures can be classified by the irreducible representations (IR) of the symmetry group of the crystal in the paramagnetic phase. The results of the symmetry operations are summarized in Table 1 where the first column contains irreducible representations of the $P2_1/c$ space group; corresponding symmetry operations and basis vectors of magnetic structure and permutation symmetry of magnetic modes are listed for each modification separately. Note, that different topologies of magnetic chains in both compounds lead to a different content of Table I for α- and β-modifications.

For a uniform magnetic order in a monoclinic Heisenberg magnet, only one basis vector describes the magnetic structure in exchange approximation since the leading isotropic exchange is much stronger than DM and anisotropic interactions. In the case of a four-sublattice magnet, the average magnitude of such a vector in the ordered state will be close to 4*S*, while the others belonging to the same irreducible representation will be smaller by order of *D*/*J*.

Table 1. Symmetry of magnetic modes in α-$TeVO_4$ and β-$TeVO_4$

$C_{2h}(2/m)$	1	2_y	I	m_y	α-$TeVO_4$		β-$TeVO_4$	
A_g	1	1	1	1	L_{1x}, F_y, L_{1z}	**F**	L_{3x}, F_y, L_{3z}	**F**
A_u	1	1	–1	–1	L_{2x}, L_{3y}, L_{2z}	$\mathbf{L}_3$	L_{1x}, L_{2y}, L_{1z}	$\mathbf{L}_2$
B_g	1	–1	1	–1	F_x, L_{1y}, F_z	$\mathbf{L}_1$	F_x, L_{3y}, F_z	$\mathbf{L}_3$
B_u	1	–1	–1	1	L_{3x}, L_{2y}, L_{3z}	$\mathbf{L}_2$	L_{2x}, L_{1y}, L_{2z}	$\mathbf{L}_1$

As apparent from Table I, the components of the $\mathbf{L}_2$ and $\mathbf{L}_3$ vectors and the ferromagnetism vector **F** do not coexist in the same irreducible representation in α-$TeVO_4$. This implies that weak ferromagnetism is incompatible with uniform AFM ordering in the chains of α-$TeVO_4$. A detailed investigation of the exchange paths in the chain network shows that intrachain DM interaction is absent for the given chain. For the $\mathbf{L}_1$ type Néel state with AFM order of nonzero ferromagnetic moments **m** on neighboring chains, the weak ferromagnetism should appear only due to interchain interactions. Note that the zigzag-like geometry makes interchain interaction along the *c* axis strongly asymmetric and frustrated in α-$TeVO_4$.

In contrast, in β-$TeVO_4$ there is no uncertainty with the intrachain exchange interaction which is apparently AFM type at low temperatures. Therefore just components of the $\mathbf{L}_2$ and $\mathbf{L}_3$ vectors should be considered as order parameters for possible uniform magnetic order. Another distinc-

tive feature is the presence of strong intrachain Dzyaloshinskii–Moriya interaction with the resulting DM vector lying in the *ac* plane (see Fig. 1,*d*) due to the topology of the V–O–V exchange pathway. As follows from the Table 1 every component of the $\mathbf{L}_3$ type order parameter should generate weak ferromagnetism. However, no remanent magnetization has been detected at low temperatures [8]. Thus, we conclude that only the $\mathbf{L}_2$ type AFM order persists in β-$TeVO_4$. This type of AFM order implies a FM interchain interaction that is also supported by experiment [8] in which weak ferromagnetic interchain correlations were detected. Furthermore, the anisotropy of the *g*-tensor with $g_b > g_a, g_c$ as well as anisotropy of the magnetic susceptibility [8] both suggest that the main AFM order parameter is L_{2y}. In accordance with Table I this type of order is accompanied by weak antiferromagnetic components L_{1x} and L_{1z}. The respective contribution of the intrachain DM interaction to the Hamiltonian (2) has the following form:

$$H_{DM} = D_x[(L_{2y}L_{1z} - L_{2z}L_{1y}) + (L_{3y}F_z - L_{3z}F_y)] + \\ + D_z[(L_{2x}L_{1y} - L_{2y}L_{1x}) + (L_{3x}F_y - L_{3y}F_x)]. \quad (5)$$

Here D_i ($i = x, y$) are components of the Dzyaloshinskii–Moriya vector. Note that if the $V–O_{ap}$ distance increases the *z* component of the DM vector decreases.

One can demonstrate that any kind of uniform antiferromagnetic order will be unstable against the creation of incommensurate spin-density waves in both α- and β-$TeVO_4$ compounds. This is described by Lifshitz invariants which are allowed in these compounds even in exchange approximation. The microscopic origin of these invariants results from competing interactions and frustration. However, in β-$TeVO_4$ strong uniform and nonuniform intrachain DM interactions create additional mechanisms for development of incommensurate magnetic structures. The possibility of a magnetic phase transition from a uniform to an incommensurate magnetic state in the β-$TeVO_4$ has been supported by the observation of distinctive features in the magnetic susceptibility at 2.26 and 3.28 K [8]. Meanwhile, in α-$TeVO_4$ no such features have been observed in magnetic susceptibility up to 1.8 K [7].

3.4. Phonons

Selected polarized Raman spectra of α- and β-$TeVO_4$ measured at temperatures of 290 and 5 K are shown in Fig. 3. The narrow linewidth of the observed phonon modes indicates the high quality of our single crystals. The monoclinic ($P2_1/c$, $Z = 4$) crystal structure of $TeVO_4$ with all atoms having a site symmetry of 4*e* leads to $\Gamma = 18A_g+18B_g+17A_u+16B_u$ Raman- and infrared-active phonon modes. The corresponding Raman tensors are given by:

$$A_g = \begin{pmatrix} a & d & 0 \\ d & b & 0 \\ 0 & 0 & c \end{pmatrix}, \quad B_g = \begin{pmatrix} 0 & 0 & e \\ 0 & 0 & f \\ e & f & 0 \end{pmatrix}.$$

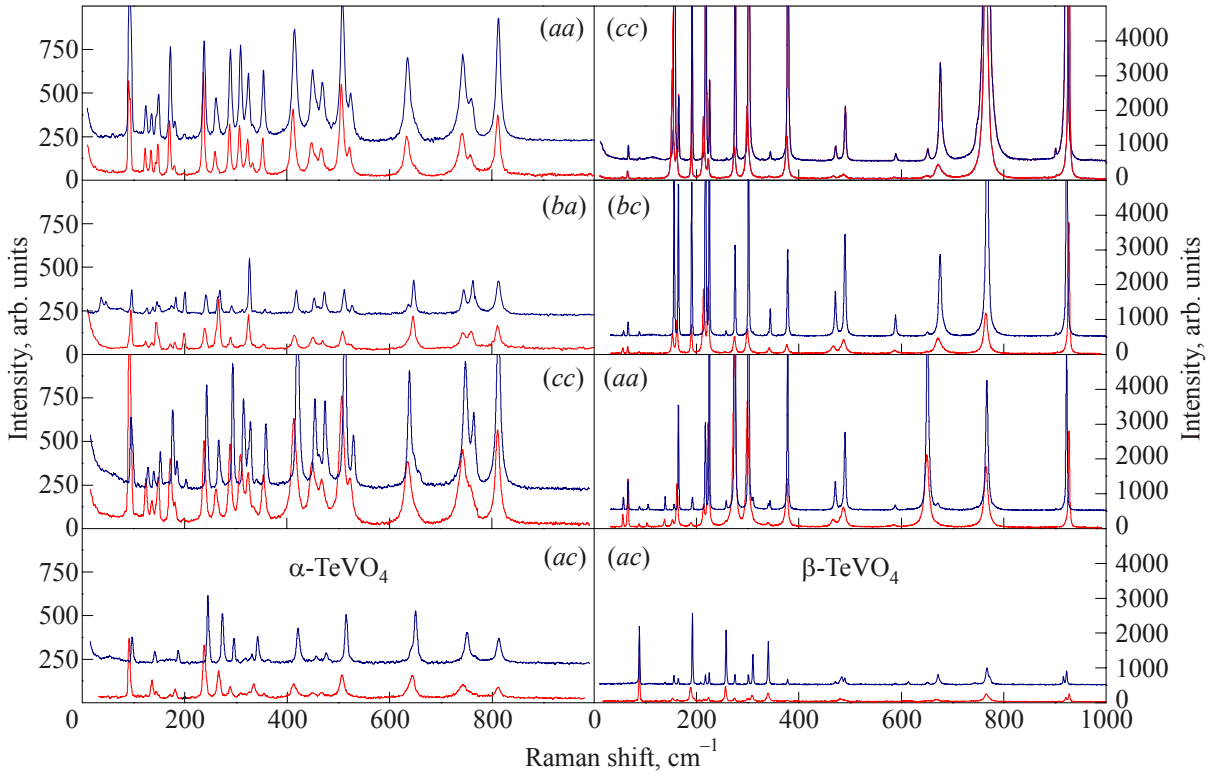

Fig. 3. Raman spectra of α- (left) and β-$TeVO_4$ in different selected polarizations taken at 290 and 5 K. Low-temperature spectra are shifted vertically for clarity.

Experimentally, in the frequency region of 10–1000 cm^{-1}, 32 (36) Raman-active phonon modes were identified in the spectra of α-$TeVO_4$ (β-$TeVO_4$). We will focus on the temperature dependence of the phonon frequencies, linewidths, and intensities extracted by fitting the corresponding spectra to Lorentzian profiles. The results are summarized in Fig. 4. With decreasing temperature several distinctive features show up for both samples:

α-$TeVO_4$. Upon cooling from room temperature all modes undergo a hardening and then saturate in frequency around T^* (Fig. 4,*a*). Upon further cooling they show a jump around $T = 50$ K and further hardening at lower temperatures. The linewidths of the phonons show an anomalous behavior at temperatures below T^* especially for the low energy modes (Fig. 4,*b*). Normally, phonon linewidths narrow monotonously with decreasing temperatures. The integrated intensity of phonon lines shows an anomalous behavior (Fig. 4,*c*) as well.

β-$TeVO_4$. All phonon modes (except for the line at 927 cm^{-1}) show a similar behavior: upon cooling their frequencies increase nearly monotonously (Fig. 4,*d*) due to lattice contraction. The anomalous temperature dependence of the frequencies starts at around $T_c^{\beta\text{-}TeVO_4}$, below which frequencies decrease. We want to note that small anomalies in the frequency vs T behavior are also observed near $T^* \approx$ ≈ 180 K. Moreover, in our Raman experiments T^* is higher than the corresponding temperature derived from $\chi(T)$ data measured with $H \| a, H \| c$ and coincides with the one from $H \| b$. The linewidths of all phonon lines exhibit almost normal temperature behavior (Fig. 4,*e*) which can be explained by anharmonic effects. We find that the function $\Gamma(T) = \Gamma_0 \left\{1 + d_j / \left[\exp(\hbar\omega_0 / k_B T) - 1\right]\right\}$ with d_j being a mode dependent fit parameter provides a very reasonable description of the temperature dependence of all phonon linewidths. A deviation of phonon linewidth behavior is observed only for some lines in the region of T^*. The enhanced damping in this temperature range suggests a change of the relaxation mechanism. In the respective temperature interval a modification of the exchange interactions take place. As a consequence, scattering of phonons by magnetic excitations is expected to undergo a change. In Fig. 4,*f*, the phonon intensity is plotted as a function of temperature for the three lines at 162, 299, and 927 cm^{-1}. When the temperature is lowered down to $T \approx 25$ K, the intensity of the phonons at 162 and 299 cm^{-1} strongly increases having a singularity at T^*. With further temperature decreasing, the intensity jumps up and then down at $T_c^{\beta\text{-}TeVO_4}$.

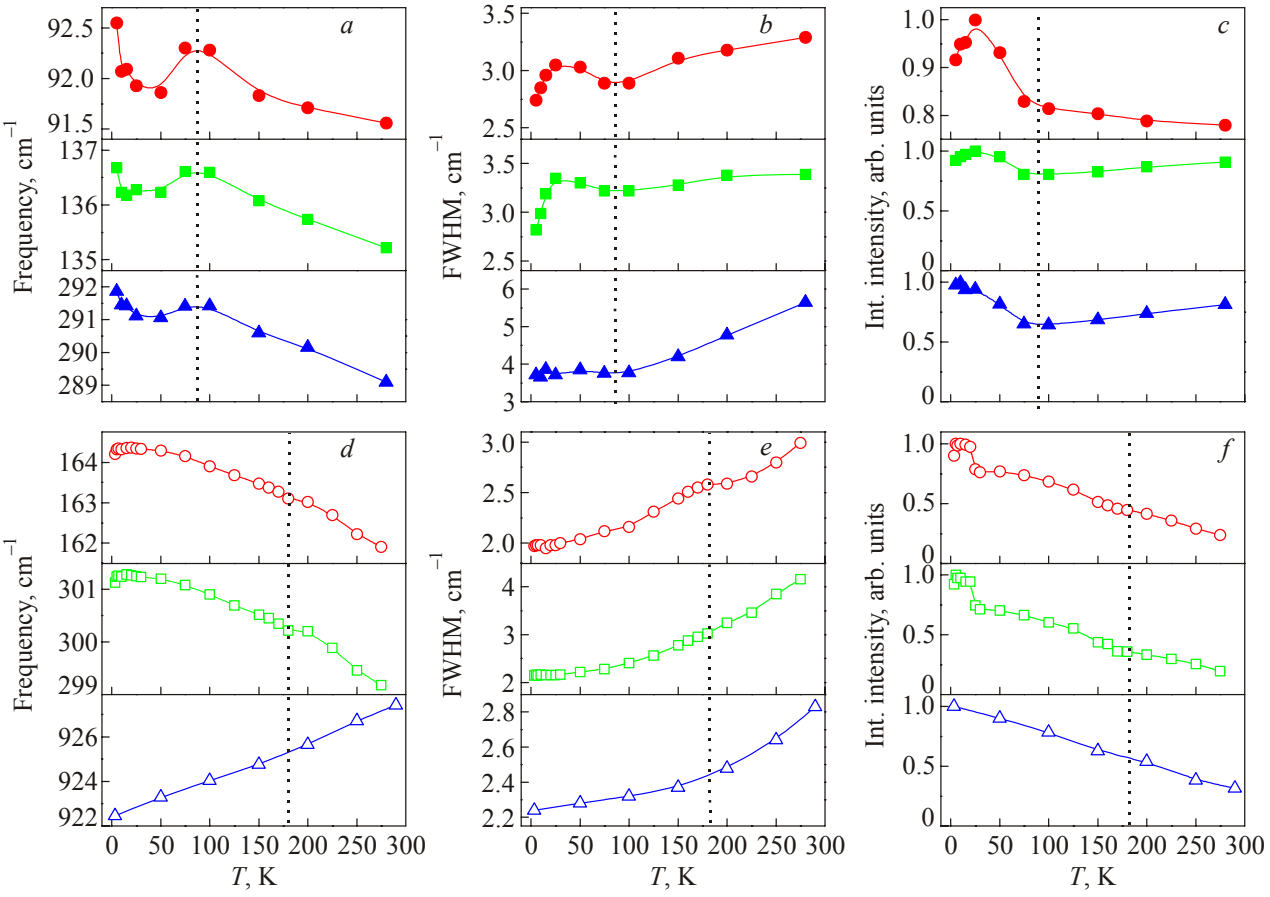

Fig. 4. Temperature dependences of the phonon frequencies (*a*, *d*), linewidths (*b*, *e*), and temperature-corrected integrated intensities of selected phonon lines in the Raman spectra (*c*, *f*) of α-$TeVO_4$ (*a*, *b*, *c*) and β-$TeVO_4$ (*d*, *e*, *f*). Dotted lines indicate the crossover temperature T^*.

The highest-frequency mode at 927 cm^{-1} represents the V–O_{ap} stretching vibrations of the apical oxygen [15]. The shorter vanadium-apical oxygen distance results in a higher mode frequency. An increase in V–O_{ap} distance may lead to a softening of this mode upon decreasing the temperature. This remarkable feature strongly supports the above mentioned scenario of the temperature induced V^{4+} shift and subsequent orbital reordering in the β-$TeVO_4$ as a reason for the FM–AFM spin-spin correlation crossover. The intensity of the 927 cm^{-1} mode displays a strong increase in the whole temperature range down to lowest T without saturation. The absence of singularities, correlated with anomalies in magnetic properties, indicates that this phonon is not involved in the magnetic exchange pathways.

Summarizing, the characteristic temperatures at which anomalies in magnetic susceptibility and specific heat are seen are also evident in the phonon spectra. This gives evidence for spin-phonon coupling in both compounds, α- and β-$TeVO_4$. It is also seen from the Fig. 4 that the spin-phonon coupling is manifested to a greater extent in the spectra of α-$TeVO_4$.

3.5. Magnetic Raman scattering

Magnetic excitations in α- and β-$TeVO_4$ are expected as quasielastic scattering, structured background, and distinct finite-energy modes. They can be identified in the Raman spectra through their temperature and polarization dependences. In magnetic systems quasielastic scattering is a very general feature. It may originate from spin diffusion [16,17] or fluctuations of the energy density of the spin system [18]. The former mechanism is forbidden in perfect 1D spin systems and leads to a Gaussian line shape [19] of the central line, while the latter leads to a Lorentzian [18], and is important for systems with nonnegligible spin-phonon coupling. Spin-phonon coupling leads to an enhancement of the spectral weight of the energy fluctuations by reducing their time scale [20]. A difference in magnitude but non-negligible spin-phonon interactions evidenced by phonon anomalies (see Fig. 4) strongly suggest that the quasielastic scattering in α- and β-$TeVO_4$ originates from energy fluctuations.

The temperature evolution of the quasielastic scattering measured in two scattering geometries for α-$TeVO_4$ is shown in Fig. 5,*a*,*b*. Note that the Lorentzian spectral function is in very good agreement with our observed quasielastic lineshape. In all our experiments the Raman setup was suitably adjusted so that Rayleigh scattering is suppressed for frequencies above 10 cm^{-1}, and the observed scattering is therefore intrinsic. Much attention was also paid to the quality of the sample surfaces.

In accordance with the scattering Hamiltonian of a 1D spin system, quasielastic scattering should only be ob-

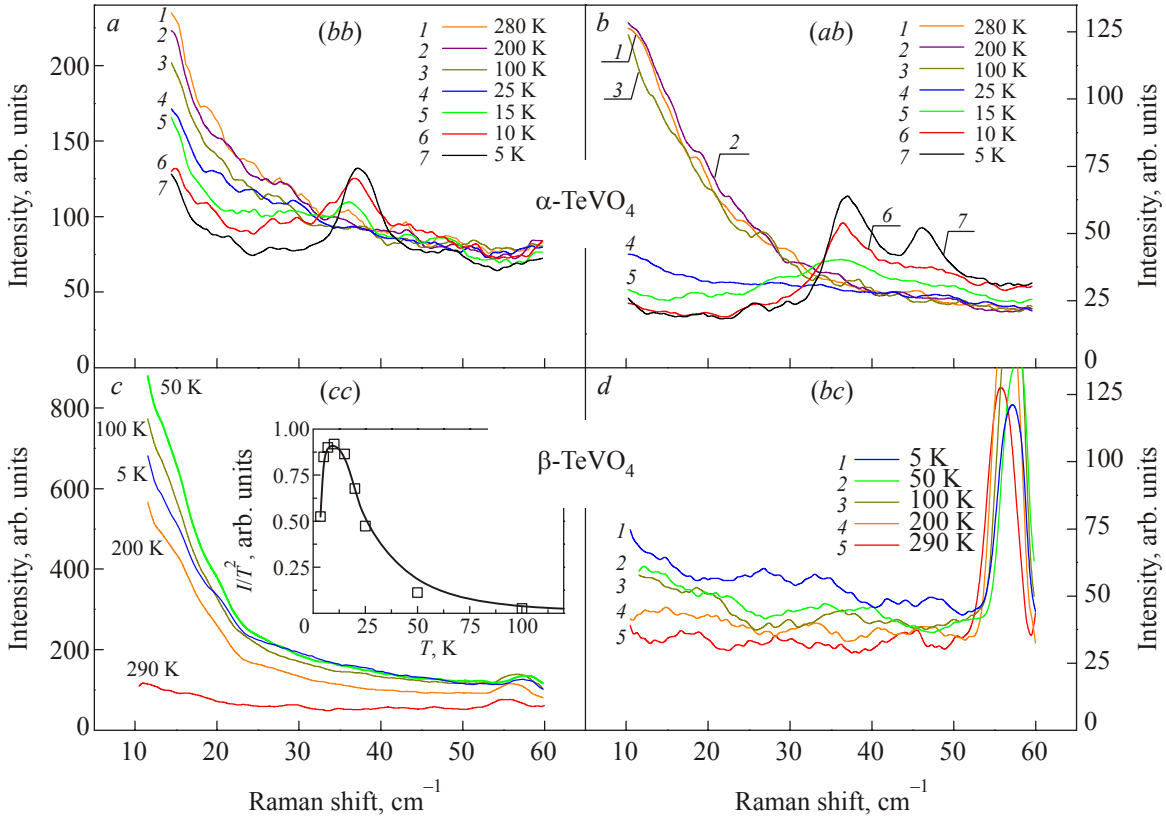

Fig. 5. (Color online) Magnetic quasielastic scattering in α-$TeVO_4$ that evolves into finite-energy modes for low temperatures in (*bb*) intrachain and (*ab*) crossed light polarizations (*a*,*b*). The same for β-$TeVO_4$ (*c*,*d*). The inset in (*c*) shows the magnetic specific heat derived from quasielastic scattering.

served in intrachain scattering configuration, i.e., with the incident and scattered light polarizations parallel to the chain direction. Experimentally this is not the case for α-$TeVO_4$ as this signal is observed with even stronger intensity in crossed polarizations. This violation of the selection rules can be attributed to the orientation of the nearest-neighbor V–V bonds and V–O–V–O planes (see Fig. 1,*b*) that alternate. The chains are distorted into a zigzag shape with an effective direction along the *b* axis. A deflection of V–V exchange paths from the *b* direction leads to a violation of the light-scattering selection rule as it is governed by local hopping processes. We note a similar infringement e.g. for the spin-chain compound $(VO_2)P_2O_7$ [21].

For the intrachain (*bb*) and interchain (*aa*) scattering configurations, the quasielastic Raman response in α-$TeVO_4$ decreases smoothly with lowering temperature (Fig. 5,*a*). In the crossed polarization (*ab*) there is an abrupt decrease in the scattering intensity at the crossover temperature T^* (Fig. 5,*b*) and a possible further decrease for $T < T^*$. These effects were attributed to sudden changes in the energy density fluctuations [7] and will be discussed below.

In Fig. 5,*c*,*d* Raman spectra of β-$TeVO_4$ display quasielastic scattering as function of temperature. As was expected, a notable contribution was observed only in the intrachain (*cc*) configuration. Quasielastic scattering increases upon temperature lowering up to 25 K and decreases at further cooling. We should note that the quasielastic scattering of very low intensity was also observed for β-$TeVO_4$ in the crossed (*bc*) geometry (Fig. 5,*d*) which grows in intensity at cooling. We relate the observation of quasielastic scattering in crossed geometry to a deflection of the V–V exchange paths from the *c* direction.

Quasielastic light scattering vs. temperature can be very useful to determine the magnetic part of the specific heat, C_m. According to the theory of Reiter [22] and Halley [23], the scattering intensity can be calculated using the Fourier components of a correlation function of the magnetic energy density. In the hydrodynamic conditions and for high temperatures this function can be simplified leading to a Lorentzian profile $I(\omega) \propto C_m T^2 D_T k^2 / [\omega^2 + (D_T k^2)^2]$, where k is the scattering wave vector, D_T the thermal diffusion constant, and C_m the magnetic specific heat. From this equation, C_m is proportional to the scattering integrated intensity divided by T^2. Such analysis was performed for a number of low-dimensional magnets [24–26]. The inset in Fig. 5,*c* shows the magnetic specific heat derived from the quasielastic scattering.

The phonon modes in Raman spectra of α-$TeVO_4$ at $T > T_c$ are superimposed onto a structured temperature- and symmetry-dependent background. The large width of the observed signal distinguishes it from the comparably sharp phonon lines. Raman-active transitions between crystal split d levels of the V^{4+} ions should have a larger energy [27,28] and are not responsible for the observation either. Besides, the temperature evolution of the background signal does not reflect the discrete nature of excitations between well-defined atomic electronic levels. We therefore assume magnetic excitations and the corresponding two-magnon Raman-scattering process as its origin, similar to other chain systems [29,30].

In the model proposed in Ref. 7 the ground state of α-$TeVO_4$ is given by a spin singlet with low-energy gapless spinonlike excitations. In the case of isotropic 1D $S = 1/2$ Heisenberg chains the elementary excitations are spinons — gapless domain wall solitons. Their dynamical structure factor is given by a two-particle continuum restricted by a lower, $\omega_q^l = \pi/2 J |\sin(q)|$ and an upper, $\omega_q^u = \pi J |\sin(q/2)|$ dispersing boundary [31,32]. Light scattering leads to total spin-zero excitations with total momentum $k = 0$, e.g., two- or four-spin excitations. As the spectral weight for two spinons at $k = 0$ vanishes the excitation spectrum consists of four-spin excitations with $k = 0$ and an energy range up to $\omega = 2\pi J$. With alternation δ of the coupling constants to nearest neigbors, $J_{NN}^{\pm} = (1 \pm \delta) J_{NN}$ along the chain or a sufficient degree of frustration, $\alpha = J_{NNN}/J_{NN} \geq 0.2412$ due to NNN exchange, a quantum phase transition from a gapless critical state into a gapped state (disordered spin liquid) is induced by dimerization. In the dimerized phase (purely magnetic 1D model) the excitations can be considered as local triplet and a corresponding two-particle continuum of triplet excitations. If a frustration of the spin system due to NNN intrachain exchange or an interchain interaction is taken into account, well-defined magnetic bound states also develop [33–35].

Numerical calculations of the Raman intensity corresponding to the four-spinon excitations for the 1D spin-1/2 model in the parameter range of $-0.5 \leq J_{NNN}/J_{NN} \leq 0.5$ reveal a broad continuumlike feature [36] (Fig. 6,*c*). A comparison of these results with our Raman spectra of α-$TeVO_4$ in (*aa*) and (*bb*) scattering geometries leads to qualitative agreement supporting the intuitive attribution of the $T > T_c$ continuum to multi-spinon scattering. In a strictly 1D system, the Fleury–Loudon polarization selection rules [37] do not allow coupling a perpendicular electronic polarization, e.g., the (*aa*) scattering configuration, to the chain direction. The observed scattering in (*aa*) and (*bb*) geometries is therefore attributed to the bent exchange path with contributions both parallel and perpendicular to the crystallographic *b* axis. In (*ab*) polarization we observe only a featureless high-temperature Raman band at around 100 cm^{-1}. This effect is attributed to the different form factor and the much weaker two-dimensional correlations that contribute to this scattering polarization. As an example we refer to the polarization dependence of the magnetic scattering in the 2D cuprates [38,39].

Figure 6,*a*,*b* displays the temperature dependence of the magnetic scattering, i.e., its evolution from broad continua to sharper modes at $T < T_c$ and anomalies for $T_c < T < T^*$. We note a few peculiarities regarding these spectra: (i) the

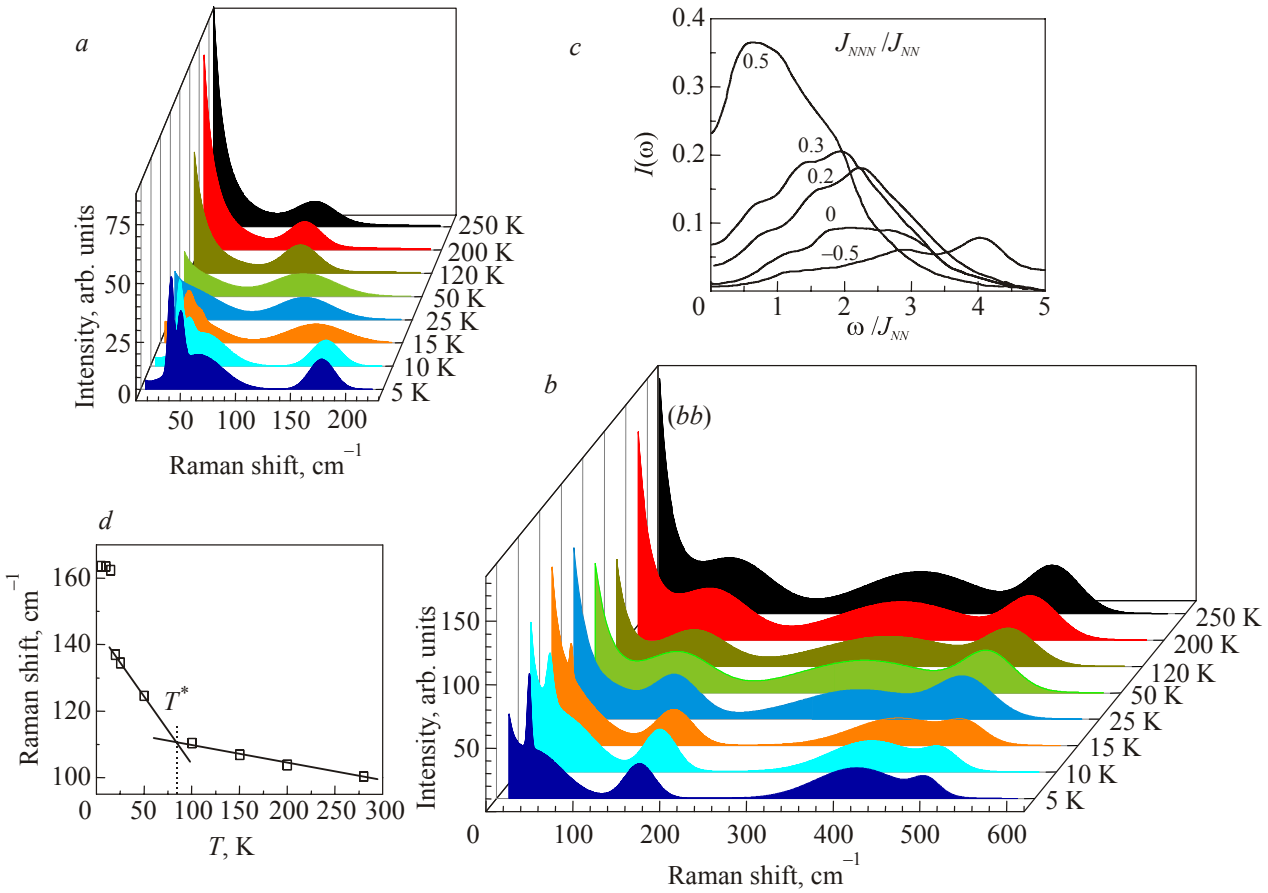

Fig. 6. (*a*,*b*) — Temperature variation in the magnetic Raman scattering in α-$TeVO_4$. (*d*) — The temperature dependence of the frequency position of the band at ~100 cm^{-1} in (*b*). (*c*) — Raman intensity for the Heisenberg model ($H = J_{NN} \sum_{(i,j)=NN} \mathbf{S}_i \cdot \mathbf{S}_j + J_{NNN} \sum_{(i,j)=NNN} \mathbf{S}_i \cdot \mathbf{S}_j$) for various ratios of NNN exchange J_{NNN} to NN exchange J_{NN} from Ref. 36.

shift with cooling of the Raman band in the 100 cm^{-1} region to higher frequencies; (ii) the shift of a band in the 300 cm^{-1} region to higher frequencies and its broadening; (iii) the temperature independence of position and width of the band around 450 cm^{-1}. Theoretical modeling (see Fig. 4 in Ref. 31) shows that with decreasing temperatures the spectral features in the magnetic continuum shift to higher frequencies. This is roughly consistent with our experimental observations.

The temperature dependence shown in Fig. 6 correlates also with the characteristic temperatures obtained from magnetic-susceptibility and specific-heat measurements. In particular, the peak position of the band at 100 cm^{-1} hardens linearly with cooling with an abrupt change in the slope at T^* = 85 K (see Fig. 6,*d*). Besides this, its bandwidth changes noticeably with crossing T^*: it decreases in (*bb*) and (*aa*) geometries and increases in (*ab*) geometry. These observations together with the modeling of magnetic Raman continua as a function of J_{NNN}/J_{NN} (Fig. 6,*c*) allow us to suggest that the crossover temperature T^* is related to a modification of the exchange interaction along the zigzag chain. This process is also related to the phonon anomalies observed at T^* and indicates the relevance of magnetoelastic coupling. Nevertheless, long-range structural distortions for $T < T^*$ are not supported by the data as no new phonon modes are observed. On the other hand all ions are located at the general 4*e* positions with identity being the only symmetry operation; i.e., shifts of the ions in the primitive cell do not violate space symmetry. The chain geometry implies that shifts which modify the critical V–O–V bond angle would lead to a change in the slope of $\chi^{-1}(T)$. Possible displacements are an increase of the O1–O1′ distance (2.4 Å above T^*) which is the shortest oxygen–oxygen distance and shifts of the vanadium ions which reduce the alternation of short and long V–V intrachain distances. These distortions are depicted in Fig. 1. In spite of the similar influences of O1 and V1 shifting on the V–O–V bond angles, they lead to different changes in components of the *g* factor.

In the case of β-$TeVO_4$ we propose a more straightforward mechanism for the change in the slope of $\chi^{-1}(T)$. It is based on the orbital reordering induced by V^{4+} ions moving away from the apical oxygen. As evidenced from the continuous softening of the 927 cm^{-1} mode this movement persists down to lowest temperature. As mentioned above it does not change the orbital state below a critical V–O_{ap} distance (i.e. below T^*). However, it decreases the distance between V^{4+} and apical oxygen from the nearest VO_5 py-

ramidal complex along the *a* axis, placing the 1D magnetic system close to 3 dimensionality. We propose that around 25 K the V–O_{ap} distance (next pyramids) reaches a critical value, at which interchain exchange interaction along *a* axis becomes important. Note, that in the proposed scenario only the phonon mode at 927 cm^{-1} is involved and demonstrated frequency anomaly.

In contrast to α-$TeVO_4$, no continuum that can be attributed to multi-spinon excitations was found in Raman spectra of β-$TeVO_4$. For the proposed uniform AFM exchange coupling with the *single* NN intrachain antiferromagnetic interaction [8], there would be no magnetic scattering within the Fleury–Loudon scheme [37,40], as the scattering operator would commute with the spin Hamiltonian (2). However, phonon induced spin exchange [41] would add a NNN term in the system Hamiltonian. On the other hand, calculations have shown [36] (see Fig. 6,*c*) that in this case the intensity of multi-spinon Raman scattering is rather small.

Figures 5 and 6 show that the Raman spectra of α-$TeVO_4$ demonstrate drastic changes also at low frequencies and temperatures below 16 K: (i) two sharp peaks appear around 37 and 47 cm^{-1} and (ii) a peak appears at 68 cm^{-1} (see inset in Fig. 7) with a linewidth of ~35 cm^{-1}. The latter feature is present in parallel and crossed polarizations with different peak intensities. The temperature dependence of the signals is analyzed in detail in Fig. 7. The higher-frequency mode is renormalized but persists well into the paramagnetic state up to ~3T_c. A very similar observation has been made in the helically ordered spin-chain systems $LiCu_2O_2$ and $NaCu_2O_2$ and interpreted as two-magnon (TM) scattering and damping of short-range spin correlations by thermal fluctuations [42,43]. The low-energy peaks at 37 and 47 cm^{-1} are present only below the magnetic ordering temperature suggesting a one-magnon excitation as their origin. Based on their different temperature dependences, we attribute them to acoustic and optical transverse magnons at $q = 0$. For a further analysis including the higher-energy modes at 175 cm^{-1} and the double-peak feature extending from ~300 to ~550 cm^{-1}, neutron scattering and Raman scattering under external magnetic field would be helpful. The complexity of these magnetic excitation spectra is based on the helical spin correlations and the four-atom basis of the magnetic unit cell present in α-$TeVO_4$.

Shown in Fig. 8,*a* is the polarization dependence of the broad (FWHM = 28 cm^{-1}) low energy excitation seen around 112 cm^{-1} in the RS of β-$TeVO_4$. It is present in (*cc*), (*ac*), and (*bc*) scattering geometries with maximal intensity in the intrachain scattering configuration. With increasing temperature from 3.5 K (see Fig. 8,*b*) this feature undergoes a softening and damping and then disappears into a diffusive background around 25 K (~5T_c). This excitation can be interpreted as two-magnon scattering. In the classical 3D limit, the peak position of TM scattering is given by $\omega = J(2zS - 1)$, where J is the exchange constant, z is the number of NN spins, and S is the spin number [44]. Taking $J = 21.4$ K [8] one obtains $\omega = 74$ cm^{-1}. In spite of the simple estimate, the agreement is reasonable.

The evolution of the TM spectrum reflects mainly the temperature dependence of short-wavelength magnon energies and lifetimes because the TM density of states is largest at the zone boundary and long-wavelength magnons renormalize more rapidly with temperature than short-wavelength magnons [44]. In Fig. 9 the temperature dependence of the normalized TM frequency and the full width at half-maximum is presented together with 3D results [44]. Magnonpair energies of α- and β-$TeVO_4$ are renormalized only by 3% at T_N. In contrast, the magnonpair energy is renormalized by ~20% at T_N for 3D $S = 1/2$ systems. The damping does scarcely take place at T_N for β-$TeVO_4$. The higher the dimensionality is, the larger are changes of spectral weights at an energy scale comparable to the Néel temperature [42]. This is related to the fact that the Néel temperature is not an appropriate energy scale for magnetic excitations in low-dimensional systems. Compared to higher dimensional systems, the robustness of spin-fluctuation dynamics at the energy scale of T_N confirms the low-

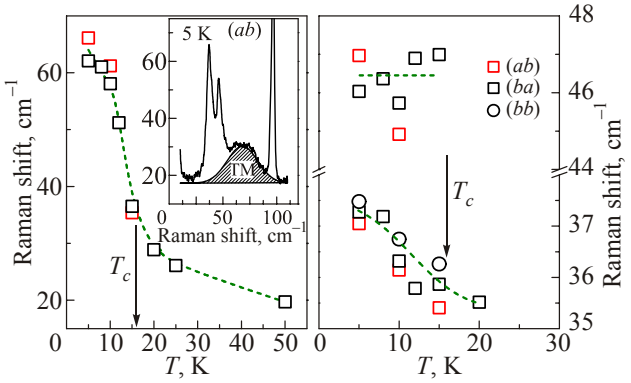

Fig. 7. Temperature dependence of the peak frequencies of the magnetic excitations in α-$TeVO_4$. Dashed lines are guides for the eyes. Inset shows the two-magnon signal in the low-temperature spectrum.

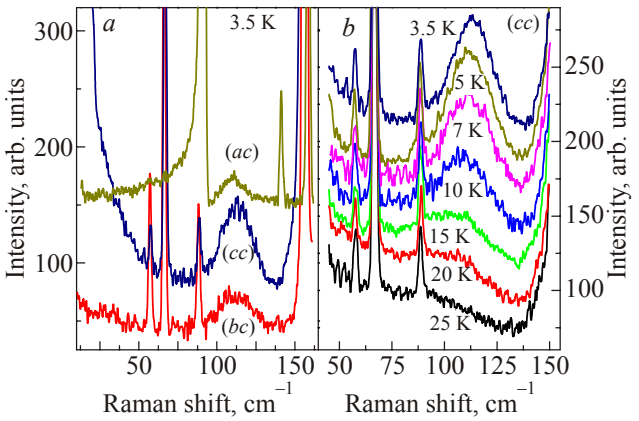

Fig. 8. Polarization dependence of the two-magnon signal in the Raman spectra of β-$TeVO_4$ (*a*) and its temperature variation (*b*).

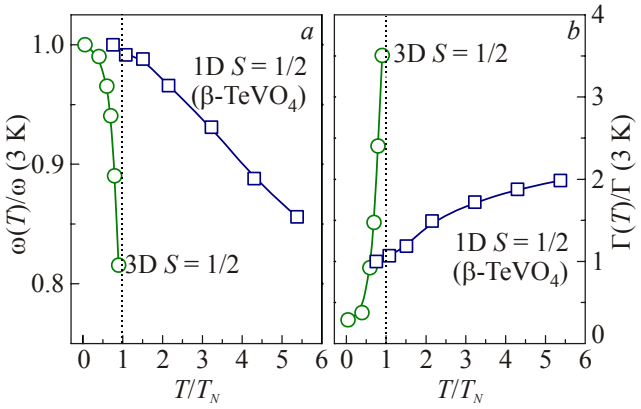

Fig. 9. Comparison of renormalized frequency (*a*) and damping (*b*) of two-magnon signal as a function of dimensionality. The higher dimensional data are taken from Ref. 44. The dashed vertical line marks a Néel temperature.

dimensional character of the studied system.

In our RS of β-$TeVO_4$ a sharp and asymmetric, fano-like phonon line at 88 cm^{-1} in (*ac*) scattering geometry is superposed on the TM band (see Fig. 8,*a*). Such asymmetry signals a coherent interaction between two scattering sources. In our case the effect is connected with an interaction between the phonon and the two-magnon excitation.

4. Conclusion

To summarize, we have presented a comparative study of the quasi-one-dimensional spin-1/2 chain systems α- and β-$TeVO_4$. These compounds, despite having the same monoclinic symmetry of the crystal lattice, differ in magnetic topology: in α-$TeVO_4$ zigzag chains parallel to the *b* axis are formed by distorted VO_6 octahedra sharing edges while in β-$TeVO_4$ zigzag chains parallel to the *c* axis are formed by slightly distorted square pyramids VO_5 sharing corners. A fit of magnetic data for both compounds was performed in terms of 1D spin-1/2 chain models [7,8]. The best qualitative agreement with the experiment was obtained for the FM alternating NN couplings and AFM NNN couplings with a weak easy-plane magnetic anisotropy in the case of the α-$TeVO_4$ and for the single AFM NN coupling for the β-$TeVO_4$. The difference in the magnetic bond topology has a pronounced influence on the intrachain Dzyaloshinsky–Moriya interaction which is absent in the α-$TeVO_4$, but present in the β-$TeVO_4$.

In both compounds substantial spin-phonon couplings lead to phonon anomalies at T^* and T_c. The FM–AFM crossover temperatures (T^* = 85/175 K for α/β-$TeVO_4$) were interpreted as temperatures at which a modification of the exchange interactions take place while at critical temperatures (T_c = 16.13/4.65 K for α/β-$TeVO_4$) a phase transition of the studied quasi-one-dimensional spin system to long-range magnetic order takes place. However, the FM–AFM crossover occurs through different mechanisms. In α-$TeVO_4$ this crossover is caused by a temperature dependent competition between FM and AFM NN exchanges along chains. In β-$TeVO_4$, on the other hand, it occurs due to orbital reordering, induced by V^{4+} ions shifting away from the apical oxygen. We conclude that a continuous increase of the V–O_{ap} distance, seen as a softening of the specific phonon mode, can drive β-$TeVO_4$ from 1D to higher dimensions at temperatures below 25 K.

The rich magnetic Raman spectrum of α/β-$TeVO_4$ was analyzed in a large temperature interval. The origin of magnetic modes was discussed. We have demonstrated in our study that interplay of spin, orbital, and lattice degrees of freedom is essential in understanding of magnetic behavior in 1D compounds.

On the occasion of his 80th Birthday we thank Prof. Victor Eremenko for his continuing interest and support of our work. V.G., Yu.P., O.A., and S.G. acknowleges finuncial support from the RFBR-NASU through the Grant No. 01-02-12(u).

1. J.B. Goodenough, *Magnetism and the Chemical Bond*, Interscience Publishers, JohnWiley&Sons, New York–London (1963).
2. P. Lemmens and K.Y. Choi, *Scattering: Inelastic Scattering Technique—Raman (Encyclopedia of Condensed Matter Physics)*, G Bassani, G Liedl, and P Wyder (eds.), Elsevier, Amsterdam (2005).
3. G. Meunier, J. Jacques, and J. Galy, *J. Solid State Chem*. **5**, 314 (1972).
4. G. Meunier, J. Jacques, and J. Galy, *J. Solid State Chem*. **6**, 67 (1973).
5. Y. Mizuno, T. Tohyama, S. Maekawa, T. Osafune, N. Motoyama, H. Eisaki, and S. Uchida, *Phys. Rev.* **B57**, 5326 (1998).
6. C. de Graaf, I. de P.R. Moreira, F. Illas, O. Iglesias, and A. Labarta, *Phys. Rev.* **B66**, 014448 (2002).
7. V. Gnezdilov, P. Lemmens, A.A. Zvyagin, V.O. Cheranovskii, K. Lamonova, Yu.G. Pashkevich, R.K. Kremer, and H. Berger, *Phys. Rev.* **B78**, 184407 (2008).
8. Yu. Savina, O. Bludov, V. Pashchenko, S. Gnatchenko, P. Lemmens, and H. Berger, *Phys. Rev.* **B84**, 104447 (2011).
9. E. Zhitlukhina, K.V. Lamonova, S. Orel, P. Lemmens, and Yu.G. Pashkevich, *J. Phys.: Condens. Matter* **19**, 156216 (2007); E.S. Zhitlukhina, K.V. Lamonova, S.M. Orel, and Yu.G. Pashkevich, *Fiz. Nizk Temp.* **31**, 1266 (2005) [*Low Temp. Phys.* **31**, 963 (2005)].
10. K.V. Lamonova, E.S. Zhitlukhina, R.Yu. Babkin, S.M. Orel, S.G. Ovchinnikov, and Yu.G. Pashkevich, *J. Phys. Chem.* **A115**, 13596 (2011).
11. Р.Ю. Бабкин, К.В. Ламонова, С.М. Орел, Ю.Г. Пашкевич, В.Ф. Мещеряков, *Оптика и спектроскопия* **112**, 483 (2012).
12. Note, that the lowering of the Z_{eff} of free ions which are placed in a crystal medium is caused by an increasing covalency and it is stronger for the ions with large valence state.

13. E.F. Bertaut, *Acta Crystallogr. Sec.* **A24**, 217 (1968); *J. Phys.* (*France*) **32**, 462 (1971); *J. Magn. Magn. Mater.* **24**, 267 (1981).
14. Yu.A. Izyumov and V.E. Naish, *J. Magn. Magn. Mater.* **12**, 239 (1979).
15. Z.V. Popović, M.J. Konstantinović, R. Gajić, V.N. Popov, M. Isobe, Y. Ueda, and V.V. Moshchalkov, *Phys. Rev.* **B65**, 184303 (2002).
16. P.M. Richards and W.J. Brya, *Phys. Rev.* **B9**, 3044 (1974).
17. W.J. Brya and P.M. Richards, *Phys. Rev.* **B9**, 2244 (1974).
18. J.W. Halley, *Phys. Rev. Lett.* **41**, 1605 (1978).
19. B.N. Narozhny, *Phys. Rev.* **B54**, 3311 (1996).
20. G.F. Reiter, *Phys. Rev.* **B13**, 169 (1976).
21. M. Grove, P. Lemmens, G. Güntherodt, B.C. Sales, F. Bullesfeld, and W. Assmus, *Phys. Rev.* **B61**, 6126 (2000).
22. G.F. Reiter, *Phys. Rev.* **13**, 169 (1976).
23. J.W. Halley, *Phys. Rev. Lett.* **41**, 1605 (1978).
24. I. Yamada and H. Onda, *Phys. Rev.* **B49**, 1048 (1994).
25. M. Grove, P. Lemmens, G. Els, G. Güntherodt, B.C. Sales, F. B'ullesfeld, and W. Assmus, *Phys. Rev.* **B61**, 6126 (2000).
26. H. Kuroe, J.I. Sasaki, T. Sekine, N. Koide, Y. Sasago, K. Uchinokura, and M. Hase, *Phys. Rev.* **B55**, 409 (1997).
27. H. Smolinski, C. Gros, W. Weber, U. Peuchert, G. Roth, M. Weiden, and Ch. Geibel, *Phys. Rev. Lett.* **80**, 5164 (1998).
28. B. Schmidt, V. Yushankai, L. Siurakshina, and T. Thalmeier, *Eur. Phys. J.* **B32**, 43 (2003).
29. P.H.M. van Loosdrecht, J.P. Boucher, G. Martinez, G. Dhalenne, and A. Revcolevschi, *Phys. Rev. Lett.* **76**, 311 (1996).
30. A. Gozar and G. Blumberg, in: *Frontiers in Magnetic Materials*, A.V. Narlikar (ed.), Springer-Verlag, Heidelberg (2005); *arXiv:cond-mat/0510192*.
31. G. Müller, H. Thomas, H. Beck, and J.C. Bonner, *Phys. Rev.* **B24**, 1429 (1981).
32. A.A. Zvyagin, *Phys. Rev.* **B73**, 104414 (2006).
33. G.S. Uhrig and H.J. Schulz, *Phys. Rev.* **B54**, R9624 (1996).
34. G. Bouzerar, A.P. Kampf, and G.I. Japaridze, *Phys. Rev.* **B58**, 3117 (1998).
35. I. Affleck, in: *Dynamical Properties of Unconventional Magnetic Systems*, A.T. Skjeltrop and D. Sherrington (eds.), *NATO ASI Series E: Applied Sciences*, Kluwer Academic Publishers, Dordrecht (1998), Vol. 349, p. 123.
36. R.R.P. Singh, P. Prelovšek, and B.S. Shastry, *Phys. Rev. Lett.* **77**, 4086 (1996).
37. P.A. Fleury and R. Loudon, *Phys. Rev.* **166**, 514 (1968).
38. R.R.P. Singh, P.A. Fleury, K.B. Lyons, and P.E. Sulewski, *Phys. Rev. Lett.* **62**, 2736 (1989).
39. F. Vernay, T.P. Devereaux, and M.J.P. Gingras, *J. Phys.*: *Condens. Matter* **19**, 145243 (2007).
40. J.B. Parkinson, *J. Phys.* **C2**, 2012 (1969).
41. B.S. Shastry and B.I. Shraiman, *Phys. Rev. Lett.* **65**, 1068 (1990); B.S. Shastry and B.I. Shraiman, *Int. J. Mod. Phys.* **B5**, 365 (1991).
42. K.-Y. Choi, S.A. Zvyagin, G. Cao, and P. Lemmens, *Phys. Rev.* **B69**, 104421 (2004).
43. K.Y. Choi, V.P. Gnezdilov, P. Lemmens, L. Capogna, M.R. Johnson, M. Sofin, A. Maljuk, M. Jansen, and B. Keimer, *Phys. Rev.* **B73**, 094409 (2006).
44. M.G. Cottam and D.J. Lockwood, *Light Scattering in Magnetic Solids*, Wiley, New York (1986).